Journal of Alloys and Compounds 509 (2011) 9836–9841

Contents lists available at ScienceDirect

Journal of Alloys and Compounds

journal homepage: www.elsevier.com/locate/jallcom

Investigation of preparation and characteristics of Sn–Bi eutectic powders derived from a high shear mechanical approach

Kun Liang[a], Xianzhong Tang[a], Lijing Yu[b], Ni Wang[a], Wencheng Hu[a,*]

[a] State Key Laboratory of Electronic Thin Films and Integrated Devices, University of Electronic Science & Technology of China, Chengdu 610054, PR China
[b] Kunming Institute of Physics, Kunming 650223, PR China

ARTICLE INFO

Article history:
Received 29 December 2010
Received in revised form 21 July 2011
Accepted 7 August 2011
Available online 12 August 2011

Keywords:
Sn–Bi alloy particles
Poly(N-vinylpyrrolidone)
Eutectic

ABSTRACT

Fusible Sn–Bi eutectic alloy particles were synthesized from bulk Sn–Bi alloy via a high-shear mechanical approach. The morphology, composition, and structure of the as-prepared Sn–Bi alloy particles were characterized by XRD, field-emission scanning electron microscopy, energy-dispersive X-ray spectroscopy, differential scanning calorimetry, thermogravimetry, and Fourier-transform infrared spectroscopy. The particles were found to be spherical and consist of the tetragonal phase of tin as well as the rhombohedral phase of bismuth. In addition, there were large amounts of poly(N-vinylpyrrolidone) coated on the particles.

1. Introduction

An increasing number of global regulations now mandate industrial goods and their manner of production to be environmentally friendly and safe to human health. Alternatives to lead-based solders for the interconnection and packaging of modern electronic components and devices are rapidly being developed [1–3]. Sn–Ag–Cu-based solders are especially popular in replacing conventional Sn–Pb alloys [4–6]. These Sn–Ag–Cu solders have good mechanical and thermal properties, and are believed to be highly reliable. However, compared with Sn–Pb solders, Sn–Ag–Cu solders have the disadvantages of poor wettability to copper surfaces, relatively high melting points, and high cost [7,8]. Energy consumption is also a noteworthy issue. The electronic assembly temperature needs to be decreased to lower the cost and the risk of production breakdown, especially of temperature-sensitive components.

Eutectic Sn–Bi solders, with their very low melting point of 139 °C, possibly meet the required parameters of step-soldering applications in conjunction with Sn–Cu–Ag Pb-free candidate solders. Sn/Bi solders have been found to outperform Sn/Pb ones in a thermal cycle test at 0/100 °C and −55/+125 °C for over 5000 cycles on organic solderability preservative boards [9]. As far as the mechanical behavior of solder joints is concerned, Sn–Bi joints are slightly stronger than Sn–Pb joints, but not at smaller elongations [10]. Other disadvantages restrict their application scope, such as the degradation of the mechanical properties of eutectic Sn–Bi alloys during thermal aging [11]. Of course, such a disadvantage can be modified by the introduction of other metals (e.g., Ag, Cu, Zn, and Ge) [12–14]. Hence, Sn–Bi solders can be an alternative powerful substitute for Sn–Pb solders, and an ideal step solder for applications with Sn–Cu–Ag candidate solders.

Screen printing is a technique that uses a woven mesh to support an ink-blocking stencil. The advantages of screen printing include versatility, short takt time, easy maintenance, environmental friendliness, and cost effectiveness [15–17]. Screen printing is appropriate for fabricating industrial-scale electrical and electronic materials due to its ability to produce thick layers from paste-like materials [18,19]. Nowadays, most electronic materials are produced via screen printing. Solder pastes are typically used to connect the leads of integrated chip packages to attachment points in the circuit patterns on a printed circuit board.

A solder paste is a thixotropic material comprising a thick medium (flux) and metal solder powder, which is the most important component. The usual solder powders currently applied include tin–silver–copper (Sn–Ag–Cu) [20], tin–antimony (Sn–Sb) [21], and tin–bismuth (Sn–Bi) [22].

Different methods for preparing metal or alloy solder powders have been proposed. Hsiao and Duh [23] have adopted a chemical reduction method to precipitate a series of Sn–Ag–Cu particles using $NaBH_4$. Huang et al. [24] have suggested the preparation of Sn–Zn and Sn–Sb powders via a mechanical alloying (MA) process. Kao and Duh [25] have used this MA method to investigate the effect of Cu concentration on the microstructure of ternary Sn–Ag–Cu solder powders. Chen et al. [26] have synthesized Sn–Bi particles in a monodispersed form by a sonochemical method. Jiang et al. [27] have reported the preparation of Sn–In solder particles and

* Corresponding author. Fax: +86 28 83202550.
E-mail address: huwc@uestc.edu.cn (W. Hu).

0925-8388/$ – see front matter © 2011 Elsevier B.V. All rights reserved.
doi:10.1016/j.jallcom.2011.08.038

bundles from a high-temperature solvent system stirred for a long time in the presence of poly(N-vinylpyrrolidone) (PVP) without any chemical reaction. Grujicic et al. [28] have introduced a cold-gas dynamic-spray process to produce solder powders and other particles.

In the present work, Sn–Bi bulk alloy was mixed with a high boiling point solvent (diethyl phthalate). The system was heated to a temperature beyond the melting point of the Si–Bi alloy (180 °C) under normal pressure to obtain fusible Sn–Bi eutectic alloy particles. Subsequently, under the mechanical impact of a high-shear force supplied by a high-shear dispersing emulsifier, the bulk was smashed to form micron-scale Sn–Bi powders with a narrow particle distribution. These Sn–Bi powders were then applied in solder pastes. To the best of our knowledge, only a few studies on the preparation of Sn–Bi alloy particles exist.

2. Experimental

Sn (99.9% pure) and Bi (99.0% pure) granules were obtained from Chengdu Chemical Works. Analytical-grade ethanol and diethyl phthalate were from the Tianjin Bodi Chemical Co. and Shanghai Chemical Works, respectively. PVP (Mw = 55,000) and analytical-grade potassium bromide (KBr) were purchased from Sigma–Aldrich Co. All the chemicals were used without further purification.

Bulk Sn–Bi alloy was obtained by melting 3.0 g Sn and 4.0 g Bi in a 20 mL vial. In a typical experiment, 1.0 g PVP and 30 mL diethyl phthalate were dissolved in a 60 mL vessel, which was placed in a 180 °C oil bath. Subsequently, 0.3 g of bulk Sn–Bi alloy was added to the vessel. The vessel was placed in a dispersing emulsification homogenizer (Model B25, Shanghai BRT Equipment Technology Co., Ltd.), which was operated under normal pressure. The rotary speed was 28,000 rpm. After 1 h, the suspension was placed in boiling water for 5 min, with a strong liquid force to shear. The suspension was then cooled down to room temperature and centrifuged at 3000 rpm for 10 min. The samples were washed with ethanol three times and dried. Samples were also prepared without using PVP.

The XRD pattern of the as-prepared Sn–Bi alloy particles was recorded by a Philips X'pert X-ray diffractometer with Ni-filtered Cu Kα radiation and a 0.15406 nm wavelength operated at 40 kV and 40 mA. Data were collected from $2\theta = 20^\circ$ to 80° at a scan rate of 0.03° per step and 0.2 s per point. Surface morphologies and particle sizes were studied using a field-emission scanning electron microscopy (FE-SEM) system (Inspect F, FEI Co.) at 20 kV. An energy-dispersive X-ray spectroscopy (EDS) instrument (EDAX Co.) was coupled to the FE-SEM system to obtain the composition of the as-prepared Sn–Bi alloy particles at 30 kV. To investigate thermal behavior, differential scanning calorimetry (DSC) was performed under a nitrogen purge of 50 cm^3 min^{-1} at a heating rate of 10 °C min^{-1} from room temperature to 500 °C on a DSC-Q 100. Thermogravimetric analysis (TGA) was performed to weigh the loss of the Sn–Bi particles at a heating rate of 10 °C min^{-1} under a nitrogen purge of 50 cm^3 min^{-1} using a TGA Q50 (TA Instruments) with an alumina crucible. The PVP capped on the as-prepared Sn–Bi alloy particles was analyzed by transmission electron microscopy (TEM; JEM-100CX, JEOL) and Fourier-transform infrared spectroscopy (FTIR; 8400S, Shimadzu Co.). The as-prepared Sn–Bi alloy particles were mixed with dried KBr and pressed to form semi-transparent pellets. The FTIR spectra were collected within 500 to 4000 cm^{-1}.

3. Results and discussion

3.1. XRD analysis

XRD was used to examine the structure of the as-prepared Sn–Bi alloy particles. Fig. 1 shows the XRD patterns of the as-prepared Sn–Bi alloy particles. In the diffraction pattern, only diffraction peaks from Sn and Bi were observed. No visible XRD peak arising from an impurity phase, such as SnO and Bi_2O_3, were found. This finding indicated that the sample formed was a Sn/Bi alloy [26].

Fig. 1 shows that (2 0 0), (1 0 1), (2 2 0), (2 1 1), (3 0 1), (4 2 0), and (3 1 2) characteristic diffraction peaks corresponding to the rhombohedral Bi texture (PDF#44-1246) with calculated lattice constants $a = b = 4.547$ Å, $c = 11.862$ Å, and $\alpha = \beta = 90^\circ$, $\gamma = 120^\circ$, located at 30.55°, 31.94°, 43.73°, 44.77°, 55.16°, 62.39°, and 79.21°, respectively, were obtained. The peaks at 27.17°, 37.93°, 39.66°, 45.79°, 48.47°, 56.01°, 59.25°, 62.12°, 64.52°, 67.31°, and 70.76° were the (0 1 2), (1 0 4), (1 1 0), (0 0 6), (2 0 2), (0 2 4), (1 0 7), (1 1 6), (1 2 2), (0 1 8), and (2 1 4) crystalline faces of the tetragonal tin texture (PDF#65-0296) with lattice constants $a = b = 5.848$ Å, $c = 3.189$ Å, and $\alpha = \beta = \gamma = 90^\circ$.

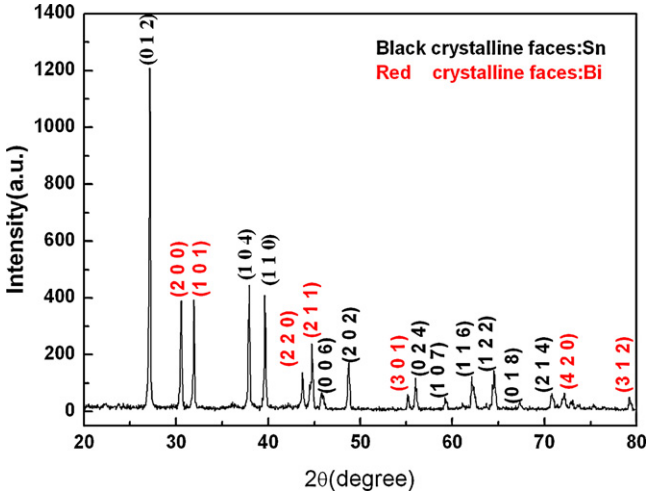

Fig. 1. XRD spectra of Sn–Bi alloy particles prepared at 180 °C for 1 h in the presence of PVP.

The lattice parameters for Sn and Bi were essentially similar with those of the bulk alloy, indicating that the as-prepared Sn–Bi alloy particles were mechanical mixtures of pure elements. According to the Debye–Scherrer formula, the average grain size of the as-prepared Sn–Bi alloy particles was estimated to be 50 nm.

3.2. SEM analysis

The morphologies of the bulk Sn–Bi alloy as well as the samples prepared with and without PVP were characterized by FE-SEM. The images are presented in Figs. 2–6. Fig. 2 shows the initial morphology of the bulk Sn–Bi alloy. Apparently, a eutectic phase was not formed, which was expected from the phase diagram. The two phases were randomly distributed, and comprised Sn-rich (dark contrast) as well as Bi-rich (bright contrast) phases.

Fig. 5 shows that the particles prepared with PVP were nearly spherical, with an average size of approximately 10 μm. The particles prepared without PVP (Fig. 6) were also spherical, with diameters ranging from 20 to 25 μm. A comparison of Figs. 3 and 4 reveals that most particles were irregular, especially in the absence of PVP. Hence, the time of preparation significantly affected the shape of the particles.

A comparison of the images of the two samples (with and without PVP) after 1 h demonstrates that the two particles were spherical. The particle sizes also decreased with PVP addition.

The FE-SEM images (Figs. 5C and 6C) of the as-prepared Sn–Bi sample show the alloy powder as agglomerates of small particles. The exact particle sizes were difficult to determine because most of the particles were aggregated. The XRD analysis shows that these spherical particles had average diameters of 50 nm.

The collision frequency Z_{AB} of two spheres can be described by the simple collision theory [29]:

$$Z_{AB} = \pi d_{AB}^2 \frac{N_A}{V} \frac{N_B}{V} \sqrt{\langle u_A \rangle^2 + \langle u_B \rangle^2} \quad (1)$$

where d_{AB} is the effective collision diameter (i.e., a summation of the radii of A and B particles), N_A and N_B are the numbers of A and B particles, respectively, and $\langle u_A \rangle$ and $\langle u_B \rangle$ are their velocities. Evidently, the maximal collision frequency occurs between a large powder (low velocity and large radius) and a small powder (high velocity and small radius) (Fig. 7).

In the preparation process of the Sn–Bi powders, the large powders were crushed by a high-shear force to form small powders

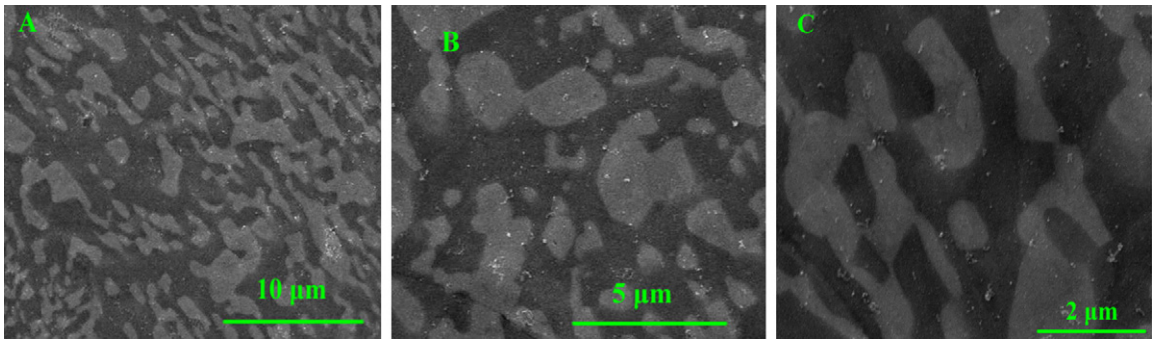

Fig. 2. FE-SEM images of the bulk Sn–Bi alloy.

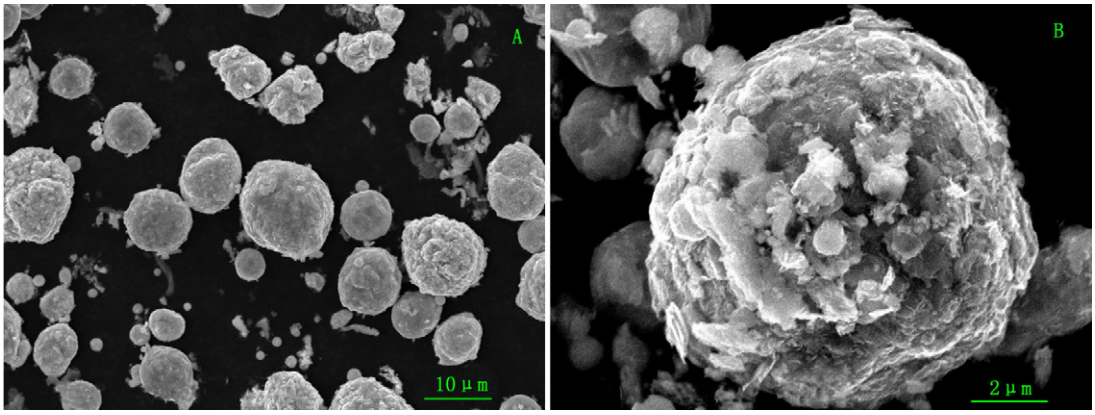

Fig. 3. FE-SEM images of the samples prepared at 180 °C for 30 min in the presence of PVP.

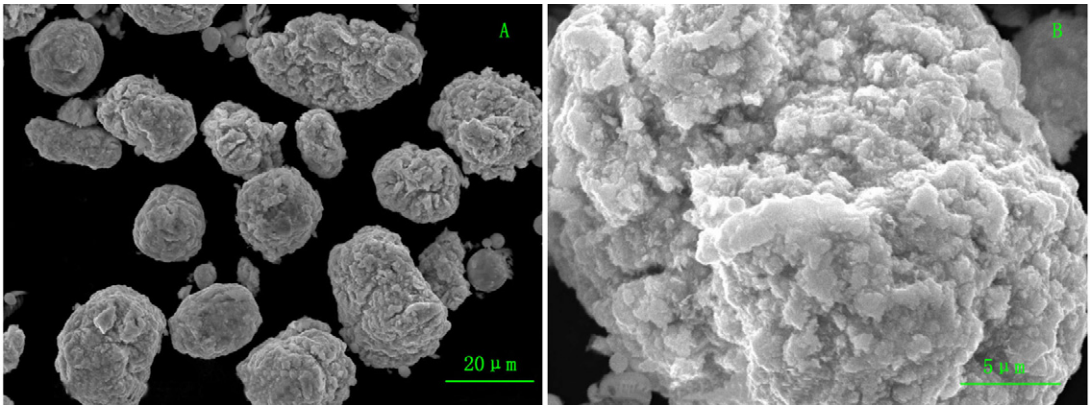

Fig. 4. FE-SEM images of the samples prepared at 180 °C for 30 min in the absence of PVP.

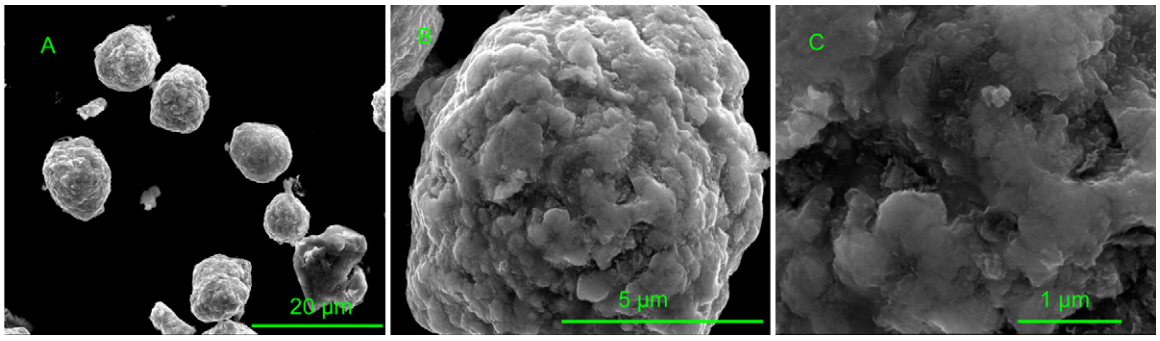

Fig. 5. FE-SEM images of the samples prepared at 180 °C for 1 h in the presence of PVP.

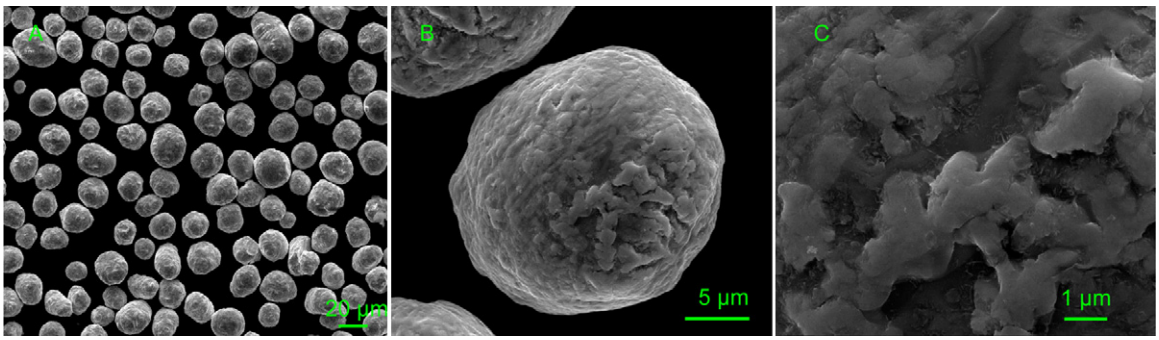

Fig. 6. FE-SEM images of the samples prepared at 180 °C for 1 h in the absence of PVP.

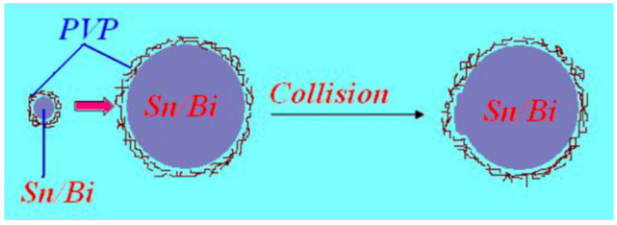

Fig. 7. Conformation change model of PVP-coated Sn–Bi alloy particles caused by collision.

with high velocities. This high-shear force caused the solvent to have a turbulent flow. Consequently, the powders collided among one another. From Eq. (1), the effective collision diameter can be regarded as the determining factor of the collision frequency.

The experimental temperature was kept beyond the melting point. Hence, every collision resulted in the combination of two powders because of their similar physical properties. When a small liquid powder collided with a large one, the former was captured and attached onto the surface of the large powder. The small powder then lost its original shape due to the tremendous impact. This phenomenon may clarify the morphologies shown in Fig. 6. Collisions between two small powders also occurred, and resulted in progressive aggregations to form large powders. When PVP was added, it was adsorbed on the Sn–Bi powder surfaces, and the surface property was hence modified. Noticeably, the combination probability decreased, suggesting the formation of relatively small Sn–Bi powders (Fig. 5).

3.3. EDS analysis

To gather further evidence on the composition of the products, EDS was performed to detect the elemental ratios. The EDS pattern shows strong Sn and Bi signals, which suggested that the Sn–Bi atomic ratio was 55.57:44.43 (Fig. 8). The weight percentages of Sn and Bi were 41.53% and 58.47%, respectively. These values are very close to the ratio of the melting points of eutectic Sn–Bi [30]. This result further supported the eutectic temperature shown in Fig. 9.

3.4. DSC-TGA

Figs. 9 and 10 display the thermal property of the as-prepared Sn–Bi alloy particles, which were studied by DSC/TGA. A sharp endothermic peak was easily observed in the DSC curves. The endothermic peaks were found at 144.63 °C in the presence of PVP, and at 143.5 °C in the absence of PVP, which were close to the eutectic temperature (139 °C) of the Sn–Bi binary alloy system [30]. This result suggested the corresponding melting point of Sn–Bi eutectic alloy particles in our experiments. The melting temperature of a solder is crucial in a soldering process, because it mainly determines the process temperature. Another endothermic peak at 340 °C was found (Fig. 9), which can be ascribed to the removal of PVP. Generally, organic molecules are bound strongly to a particle surface at an approximately monolayer coverage [31]. With increased temperature to 340 °C, PVP molecule chains are chemically cleaved to form smaller molecules under N_2 conditions, resulting in mass loss. Pure PVP begins to decompose at around 380 °C [32]. However, in the present study, decomposition occurred at 340 °C because of the PVP coated on the as-prepared Sn–Bi alloy particles. There is a 40° shift to a lower temperature, which may

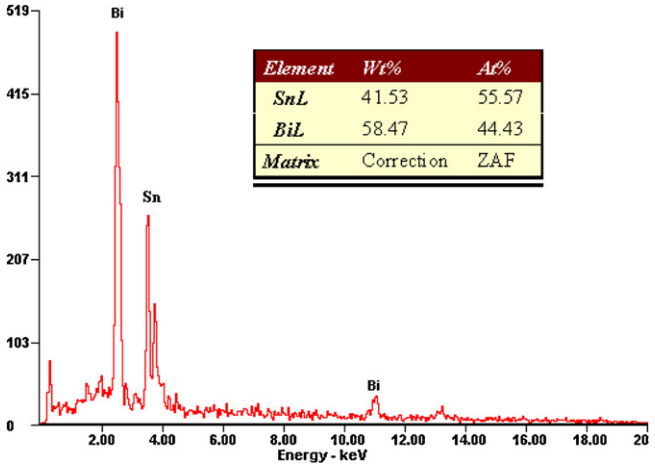

Fig. 8. EDS pattern of Sn–Bi alloy particles prepared at 180 °C for 1 h in the presence of PVP.

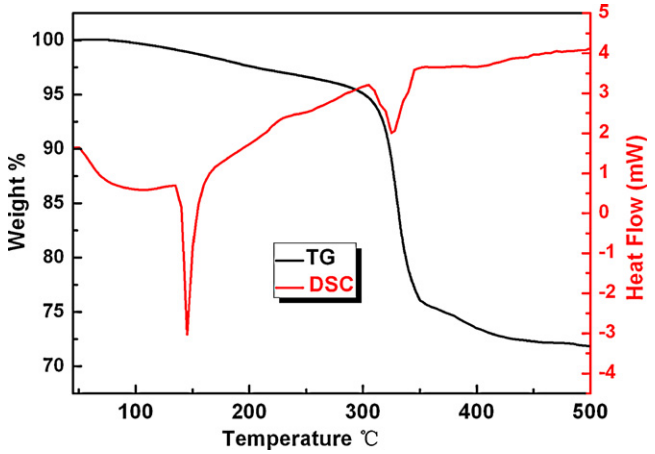

Fig. 9. DSC and TG patterns of Sn–Bi alloy particles prepared at 180 °C for 1 h in the presence of PVP.

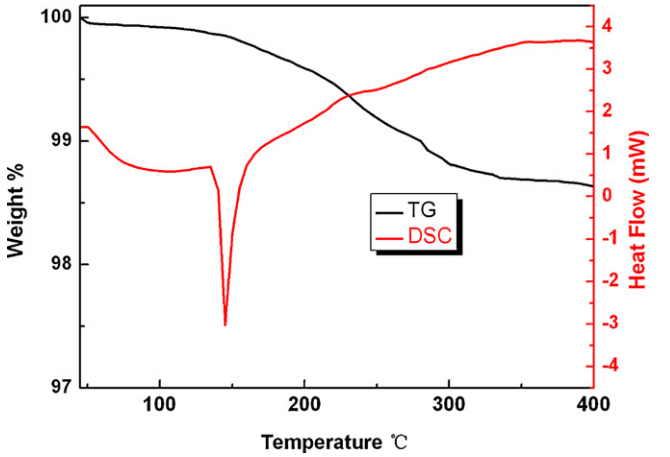

Fig. 10. DSC and TG patterns of Sn–Bi alloy particles prepared at 180 °C for 1 h in the absence of PVP.

be attributed to the alloy particles playing a catalyst role. Furthermore, the mass losses below 300 °C in Figs. 9 and 10 were due to the volatilization of ethanol and diethyl phthalate. The mass loss was only 1.2% in the Sn–Bi alloy particles prepared without PVP, whereas the mass loss was 5% in the presence of PVP. A possible reason could be the strong adsorption of PVP onto ethanol and diethyl phthalate. There was a 23% mass loss in the PVP-modified Sn–Bi eutectic alloy particles. This finding clearly showed that large amounts of PVP were absorbed on the particles at a weight ratio of Sn–Bi:PVP = 2.77:1.

3.5. TEM analysis

Figs. 11 and 12 present the TEM images of the particles prepared with and without PVP, respectively. There is no distributed phase, as presented in Fig. 9. The DSC curve only had one sharp endothermic peak at 144.63 °C, which revealed that the particles were not a simple mixture of pure Bi and Sn, but an eutectic alloy of Bi and Sn atoms.

At the same time, a circle is seen to be coated on the particles in Fig. 11, but not in Fig. 12. PVP was only applied in the first sample; hence, the material coated on the particles in Fig. 11 was the PVP, which was also confirmed by FTIR spectrum.

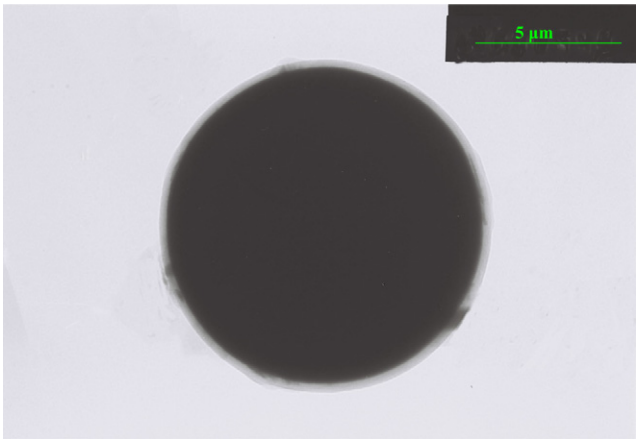

Fig. 11. TEM images of the samples prepared at 180 °C for 1 h in the presence of PVP.

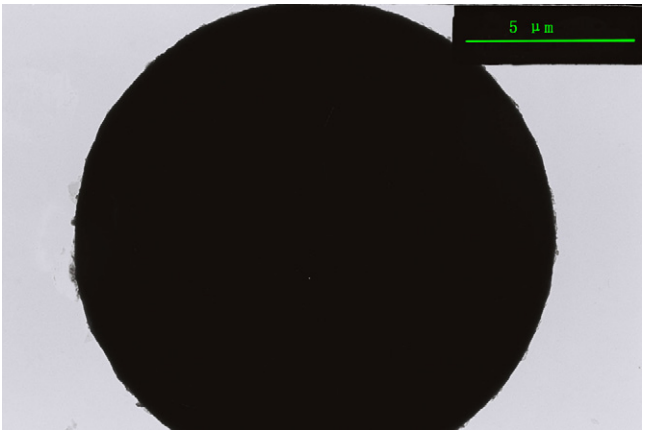

Fig. 12. TEM images of the samples prepared at 180 °C for 1 h in the absence of PVP.

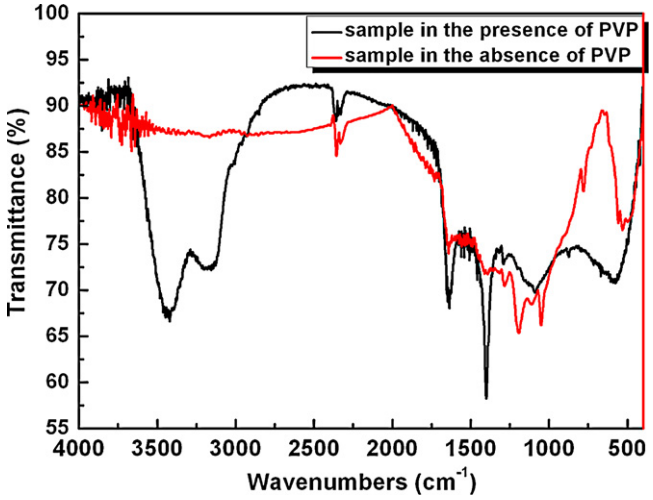

Fig. 13. FTIR of pure PVP and Sn–Bi alloy particles prepared at 180 °C for 1 h in the presence of PVP.

3.6. FTIR analysis

The IR spectrum of the as-prepared Sn–Bi alloy particles prepared in the presence of PVP is shown in Fig. 13, and is compared with those prepared without PVP. For PVP, the peak at 1679 cm^{-1} was assigned to the C=O stretching, which was very close to the previously reported 1680 cm^{-1} for PVP [33]. However, the IR spectrum of the Sn–Bi alloy particles revealed that a peak of C=O stretching shifted to 1664 cm^{-1}. This significant (15 cm^{-1}) blue shift was attributed to the coordination bonds that formed between the as-prepared Sn–Bi alloy particles and PVP molecules [34]. Therefore, the C=O bond had decreased electron density with the formation of new coordination bonds. This weakening resulted in the apparent frequency shift [35]. There was no obvious peak in the C=O bond in the spectrum of the samples prepared without PVP.

4. Conclusions

In the current paper, a high-shear mechanical approach was used to prepare fusible Sn–Bi eutectic alloy particles from bulk Sn–Bi alloy with PVP in diethyl phthalate at 180 °C under normal pressure. The morphologies, compositions, and structures of the as-prepared Sn–Bi alloy particles were characterized. The XRD pattern revealed that the particles consisted of the tetragonal phase of Sn and the rhombohedral phase of Bi. The FE-SEM images demonstrated the presence of spherical particles approximately 10 μm

in diameter for the samples prepared with PVP. The eutectic temperature was 144.63 °C on the DSC curve. The TGA, TEM, and FTIR patterns show large amounts of PVP absorbed onto the particles.

References

[1] Z. Huang, P.P. Conway, C. Liu, R.C. Thomson, IEEE Trans. Compon. Packag. Technol. 29 (2006) 98–104.
[2] S. Park, R. Dhakal, L. Lehman, E. Cotts, Acta Mater. 55 (2007) 3253–3260.
[3] J.-H. Zhao, V. Gupta, A. Lohia, D. Edwards, J. Electron. Packag. 132 (2010) 0110051–0110056.
[4] M.N. Islam, Y.C. Chan, M.J. Rizvi, W. Jillek, J. Alloys Compd. 400 (2005) 136–144.
[5] T.-H. Chuang, C.-Y. Cheng, T.-C. Chang, J. Electron. Mater. 38 (2009) 2762–2769.
[6] L. Zhang, S.-B. Xue, L.-L. Gao, Z. Sheng, G. Zeng, Y. Chen, S.-L. Yu, J. Mater. Sci. Mater. Electron. 21 (2010) 635–642.
[7] W. Falinski, H. Hackewicz, G. Koziol, J. Borecki, 27th International Spring Seminar on Electronics Technology, Bankya, Bulgaria, 2004, pp. 74–78.
[8] M.J. Kim, Y. Zhou, J.P. Jung, Solder. Surf. Mount Technol. 19 (2007) 3–8.
[9] A.Z. Miric, A. Grusd, Solder. Surf. Mount Technol. 10 (1998) 19–25.
[10] W.J. Tomlinson, I. Collier, J. Mater. Sci. 22 (1987) 1835–1839.
[11] J.F. Li, S.H. Mannan, M.P. Clode, K. Chen, D.C. Whalley, C. Liu, D.A. Hutt, Acta Mater. 55 (2007) 737–752.
[12] L. Zang, Z. Yuan, H. Zhao, X. Zhang, Mater. Lett. 63 (2009) 2067–2069.
[13] J. Zhao, L. Qi, X.-m. Wang, L. Wang, J. Alloys Compd. 375 (2004) 196–201.
[14] S.-H. Wang, T.-S. Chin, C.-F. Yang, S.-W. Chen, C.-T. Chuang, J. Alloys Compd. 497 (2010) 428–431.
[15] X. Ge, X. Huang, Y. Zhang, Z. Lu, J. Xu, K. Chen, D. Dong, Z. Liu, J. Miao, W. Su, J. Power Sources 159 (2006) 1048–1050.
[16] K. Yu, Y.S. Zhang, F. Xu, Q. Li, Z.Q. Zhu, Q. Wan, Appl. Phys. Lett. 88 (2006) 153123.
[17] V.K. Rao, M.K. Sharma, A.K. Goel, L. Singh, K. Sekhar, Anal. Sci. 22 (2006) 1207–1211.
[18] D.S. Erdahl, I. Charles Ume, IEEE Trans. Adv. Packag. 29 (2006) 178–185.
[19] J.G. Bai, J.N. Calata, G.-Q. Lu, IEEE Trans. Electron. Packag. 30 (2007) 241–245.
[20] R. Durairaj, S. Ramesh, S. Mallik, A. Seman, N. Ekere, Mater. Des. 30 (2009) 3812–3818.
[21] R. Mahmudi, A.R. Geranmayeh, M. Allami, M. Bakherad, J. Electron. Mater. 36 (2007) 1703–1710.
[22] M. Whitney, S.F. Corbin, J. Electron. Mater. 35 (2006) 284–291.
[23] L.-Y. Hsiao, J.-G. Duh, J. Electrochem. Soc. 152 (2005) J105–J109.
[24] M.L. Huang, C.M.L. Wu, J.K.L. Lai, L. Wang, F.G. Wang, J. Mater. Sci. Mater. Electron. 11 (2000) 57–65.
[25] S.-T. Kao, J.-G. Duh, J. Electron. Mater. 33 (2004) 1455–1461.
[26] H. Chen, Z. Li, Z. Wu, Z. Zhang, J. Alloys Compd. 394 (2005) 282–285.
[27] H. Jiang, K.-s. Moon, Y. Sun, C.P. Wong, F. Hua, T. Pal, A. Pal, J. Nanopart. Res. 10 (2008) 41–46.
[28] M. Grujicic, C.L. Zhao, C. Tong, W.S. DeRosset, D. Helfritch, Mater. Sci. Eng. A 368 (2004) 222–230.
[29] B.J. Orr, I.W.M. Smith, J. Phys. Chem. 91 (1987) 6106–6119.
[30] R.-K. Shiue, L.-W. Tsay, C.-L. Lin, J.-L. Ou, J. Mater. Sci. 38 (2003) 1269–1279.
[31] R.M. Riouxa, H. Songa, M. Grass, S. Habas, K. Niesz, J.D. Hoefelmeyer, P. Yanga, G.A. Somorjai, Top. Catal. 39 (2006) 167–174.
[32] Y.K. Du, P. Yang, Z.G. Mou, N.P. Hua, L. Jiang, J. Appl. Polym. Sci. 99 (2006) 23–26.
[33] H.-D. Wu, I.-D. Wu, F.-C. Chang, Polymer 42 (2001) 555–562.
[34] J. Petroski, M.A. El-Sayed, J. Phys. Chem. A 107 (40) (2003) 8371–8375.
[35] H. Jiang, K. Moon, Y. Sun, C.P. Wong, F. Hua, T. Pal, A. Pal, J. Nanopart. Res. 10 (2008) 41–46.